

Article

# Dual Thermal-/Electrical-Responsive Luminescent ‘Smart’ Window

Gilles H. Timmermans <sup>1</sup> , Robin F. Douma <sup>1</sup>, Jianbin Lin <sup>2</sup> and Michael G. Debije <sup>1,\*</sup>

<sup>1</sup> Stimuli-responsive Functional Materials and Devices, Chemical Engineering & Chemistry, Eindhoven University of Technology, 5600 MB Eindhoven, The Netherlands; g.h.timmermans@tue.nl (G.H.T.); r.f.douma@student.tue.nl (R.F.D.)

<sup>2</sup> Department of Chemistry, Xiamen University, Xiamen 361005, China; jb.lin@xmu.edu.cn

\* Correspondence: m.g.debije@tue.nl

Received: 29 January 2020; Accepted: 17 February 2020; Published: 20 February 2020



**Featured Application:** These energy management devices could be deployed as windows that automatically alter their transparency in response to changes in external temperature, with the potential for manual override by application of an electrical potential. Such windows could be of particular interest in horticultural applications.

**Abstract:** As buildings are a large energy user, it is important to not only reduce their consumption, but also have them generate their own electricity. Here, we describe a smart window that could reduce electricity consumption, normally used for air conditioning and lighting, by absorbing excess solar radiation with dichroic fluorescent dye molecules aligned in a switchable liquid crystal host and guiding the re-emitted light energy to the edges of the device, where it can be used to generate electricity via attached photovoltaic cells. The liquid crystals are responsive both to temperature changes and applied electrical fields. At higher temperatures, transmission decreases due to increased disorder in the liquid crystals, while the application of an electrical field increases transmission by effectively realigning the dyes for minimal absorption. Using alternative configurations, a window with a transparent rest state was also produced, in which transmission can be decreased by applying an electrical field; the thermal response remains identical.

**Keywords:** luminescent solar concentrator (LSC); smart window; dichroic dye; liquid crystal; electrical switching; thermal switching

## 1. Introduction

The built environment is a large consumer of electricity, with 76% being spent in residential and commercial buildings [1], around half of this on electricity for heating/cooling and lighting [2]. One way to reduce the amount of energy spent on heating and cooling is by controlling the amount of incoming sunlight using “smart windows” [3,4] which can change their transmissivity in response to stimuli, including heat [5–7], electricity [4,8,9] and light [10–12]. In addition, using excess sunlight to generate electricity can even result in energy-generating windows [13–15].

One way to fabricate energy-generating smart windows is by using the luminescent solar concentrator (LSC) concept [16,17]. LSCs are transparent lightguides, usually plastic or glass, doped with or coated with fluorescent dyes. The fluorescent dyes can absorb part of the sunlight and emit it at longer wavelengths. A significant fraction of this is trapped via total internal reflection and guided to the edges of the lightguide. By placing photovoltaic cells at these edges, the emitted light can be used to generate electricity, although the light can also be used for other applications, including daylighting [18], chemical production [19,20] or horticulture [21,22].

Recent work by Oh et al. [5] has shown that the transmission of a smart window can be thermally controlled using a dichroic dye in a liquid crystal (LC). Three different LC phases (i.e., smectic, nematic and isotropic) were used to create high-, mid- and low-transmitting states. Inspired by this system and our previous work on switchable LSCs [22,23], we show a dual electrically and thermally responsive LSC based on a fluorescent dye doped LC mixture. This system decreases its transmission with increasing temperature with a manual override that can be used to either increase or decrease the transmission by application of an electric potential, depending on the design. The edge-emitted light can then be used for the generation of electricity by attaching photovoltaic cells, or redirected for crop growth or daylighting.

## 2. Materials and Methods

Liquid crystal 8CB (4'-Octyl-4-biphenylcarbonitrile) was purchased from Synthron (Bitterfeld-Wolfen, Germany), Dye 1 (a coumarin derivative) was purchased from a commercial source, Dye 2 was synthesized according to the literature [24]; these three materials are depicted in Figure 1a.

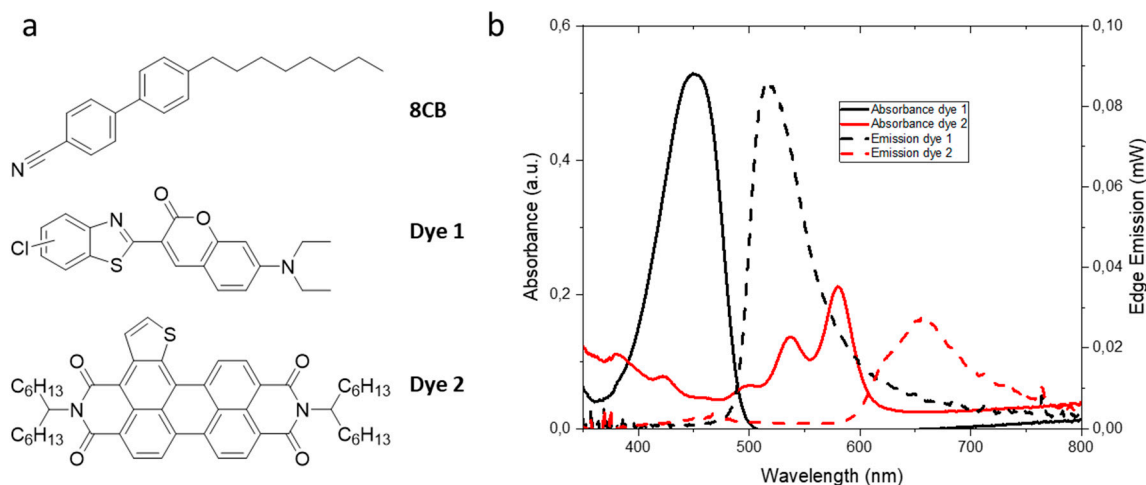


**Figure 1.** (a) The chemical structures of 8CB, Dye 1 and Dye 2. (b) Absorption (solid lines) and emission (from one edge parallel to the alignment direction, dotted lines) spectra of 1 wt% of Dye 1 (black) and Dye 2 (red) in 8CB in planar aligned 6  $\mu\text{m}$  gap cells.

Indium tin oxide (ITO)-coated glass plates of  $3 \times 3 \text{ cm}^2$  (for transmission measurements) and  $5 \times 5 \text{ cm}^2$  (for emission measurements, LC-Tec, Borlänge, Sweden) and glass plates of  $1 \times 1 \text{ cm}^2$  with ITO interdigitated electrodes (IDE), linewidth 10  $\mu\text{m}$ ; line spacing 10  $\mu\text{m}$ , (for transmission measurements) were cleaned and spincoated (Karl Suss RC-8 spin coater, 5000 rpm, 50 seconds, Garching bei Munchen, Germany) with a layer of polyimide (Optimal AL 1051, JSR corporation Tokyo, Japan, for planar alignment on the ITO-coated glass plates and Nissan Polyimide Varnish, Sunever for homeotropic alignment on the IDE samples Tokyo, Japan) and cured at 180  $^{\circ}\text{C}$  for 90 minutes; the Optimal AL 1051-coated samples were rubbed on a velvet cloth to induce planar alignment. Cells were fabricated by gluing two coated glass plates together using 6  $\mu\text{m}$  spacers. The cells were filled at  $\sim 80^{\circ}\text{C}$  with 1 wt% of either Dye 1 or Dye 2 in liquid crystal 8CB. The absorption and emission spectra for the planar devices are shown in Figure 1b.

The transmission spectra of the cells were measured using a UV-vis spectrophotometer (Perkin Elmer Lambda 750, Waltham, Massachusetts, USA); temperatures were controlled using a customized heating stage (Linkam THMS600, Tadworth, UK) and electrical potentials (AC, 1000 Hz) were applied using a laboratory function generator (Agilent 33220A, Santa Clara, California, USA) coupled to a 20  $\times$  voltage amplifier (FLC Electronics F20A, Partille, Sweden). Differential scanning calorimetry (DSC) was performed under a nitrogen atmosphere using a TA Instruments Q1000 DSC equipped with an RCS90 cooling accessory, New Castle, Delaware, USA. Polarized optical microscopy (POM)

images were made using a Leica CTR 6000 microscope equipped with a Leica DFC420 C camera, Wetzlar, Germany.

### 3. Results

The coumarin derivative (Dye 1) and perylene derivative (Dye 2) were individually dissolved at 1 wt% in 8CB. Three distinct liquid crystal phases are identified (SmA 30–35 °C N 40–45 °C I: the DSC may be found in Figure S1), similar to those found in the literature. [25].

In the planar cells, the fluorescent dyes can absorb a significant fraction of the incoming light as they are aligned with absorption axis perpendicular to the incoming light. The application of a voltage reorients the liquid crystals, which in turn reorient the dyes to a homeotropic state, to a position with the absorption axis parallel to the incoming light. Due to the dichroism of the dyes, light absorption decreases in the homeotropic orientation, resulting in a more transparent state. Increasing the temperature decreases the LC order, as seen in Table 1; the order parameters ( $S$ ) of the dyes were calculated according to [26]

$$S = \frac{A_{par} - A_{per}}{A_{par} + 2A_{per}} \quad (1)$$

where  $A_{par}$  and  $A_{per}$  are the peak absorbance when the film is exposed to light polarized parallel and perpendicular to the LC alignment direction, respectively. As the dyes become more disordered, absorption increases, as shown in Figure 2. The order parameters (see Table 1) clearly show that, as the temperature increases, the alignment of the dyes decreases as the system becomes more isotropic, finally resulting in an order parameter of 0 when the LC is fully isotropic.

**Table 1.** Order parameter of 1 wt% Dye 1 and Dye 2 in 8CB in planar cells at different temperatures.

Temperature °C	24	27	30	33	37	41
S, Dye 1	0.25	0.24	0.27	0.24	0.11	0.00
S, Dye 2	0.27	0.24	0.20	0.12	0.00	0.00

In Figure 3, transmission at the peak absorption wavelengths of the dyes at an increased temperature and voltage for planar cells are depicted: Figure 3a shows Dye 1, and Figure 3b Dye 2. Initially, in the smectic A phase at 24 °C, a higher voltage (123 Vpp (peak-to-peak voltage)) is required to overcome the LC alignment and switch the dye to a homeotropic orientation, resulting in an increased light transmission. On the other hand, increasing the temperature to the nematic state increases the mobility and disorder in the system, resulting in a lower transmission and lower switching voltage to the homeotropic state (82 Vpp at 26 °C and even 41 Vpp at 30 °C). Increasing the temperature further to the isotropic state results in a minimum transmission but prevents electrical switching, as the LC phase is randomized and loses its switching properties [27].

Emission spectra from  $5 \times 5 \text{ cm}^2$  cells from the edge parallel to the LC alignment direction were measured under a solar simulator by an integrating sphere as a function of temperature and applied voltage: the results are depicted in Figure 3c,d. It can be seen that the emissions for Dye 1 (Figure 3c) are higher compared to Dye 2 (Figure 3d). As the temperature increases, the emission parallel to the absorption increases as the transmission decreases. However, increasing the temperature too much (>35 °C) reduces edge emission as dye orientation becomes less favorable. Applying an electric potential across the cell reorients the LC/dye, at a cost of reduced emission as a result of less light absorption (even though the emission direction of the dye is more favorable).

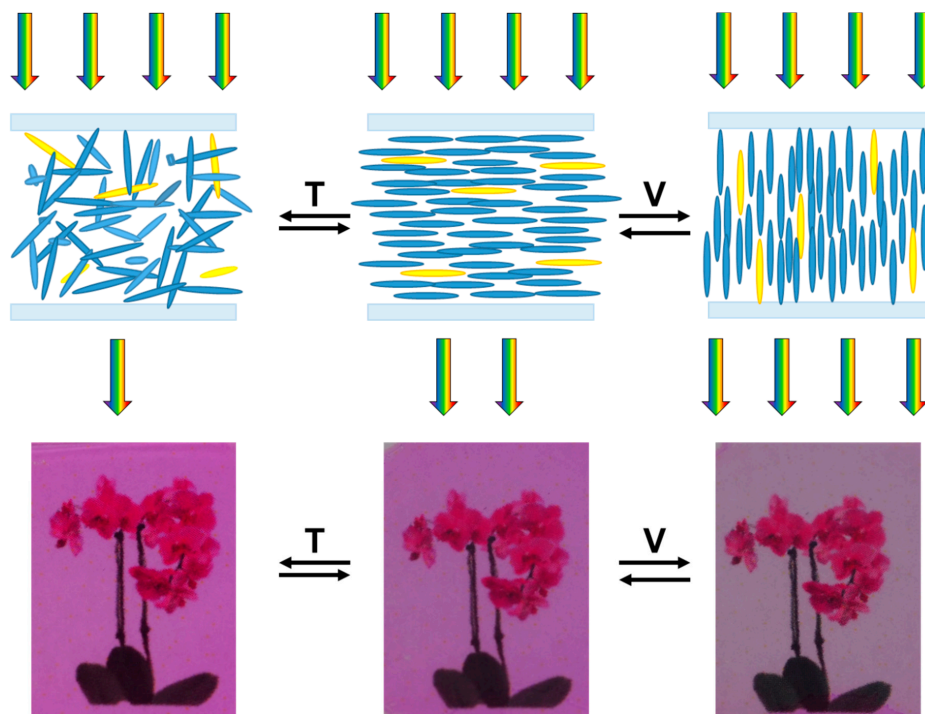


**Figure 2.** Schematic (top row) and photographs (bottom row) of liquid crystal and dye alignments in the initial planar state (middle column) and its changes upon the application of an electrical field (right column) or increased temperature (left column). The relative absorption characteristics are indicated by the rainbow-colored arrows.

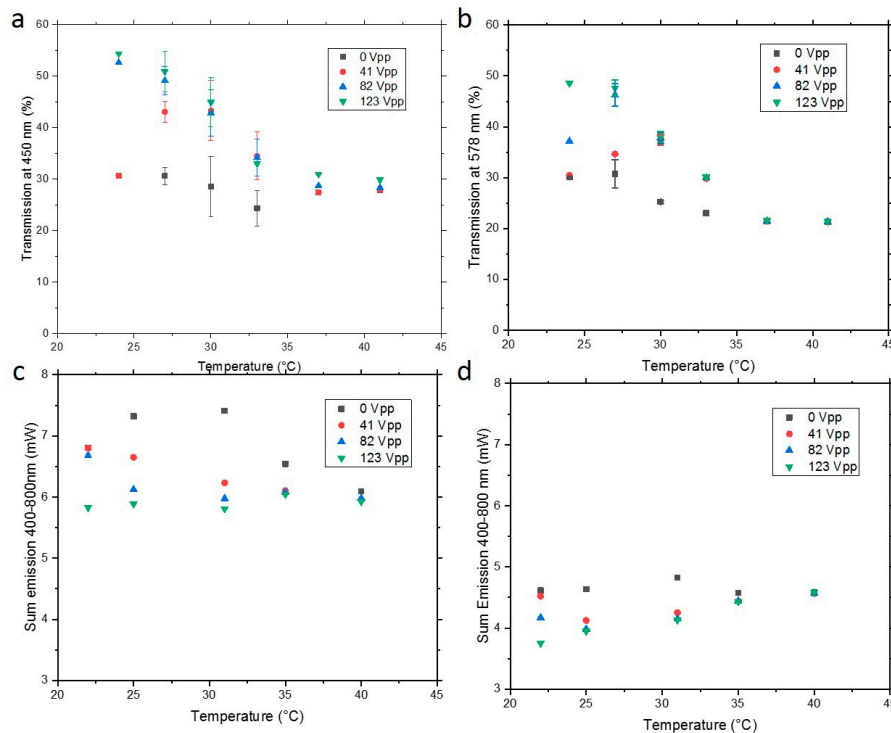


**Figure 3.** Transmission at the peak absorption of the dye at increased temperature and voltage for planar cells containing (a) Dye 1; (b) Dye 2. Summation of emission spectra (from the edge with dyes aligned parallel to the LC alignment) between 400–800 nm at increased temperature and voltage for planar  $5 \times 5 \text{ cm}^2$  containing (c) Dye 1; (d) Dye 2.

The external power efficiency ( $\eta_{ext}$ , energy emitted at the edges of the device as a function of the energy incident on the device) and the internal optical efficiency ( $\eta_{int}$ , photons emitted at the edges of the device per photons absorbed by the device) [28] of the systems at the various temperatures and applied potentials were calculated using

$$\eta_{ext} = \frac{\text{energy emitted}}{\text{incident energy}} = \frac{\int_{\text{emission}} P_{out}(\lambda_{em}) d\lambda_{em}}{\int_{sol} P_{in} d\lambda_{sol}} * 100\% \quad (2)$$

and

$$\eta_{int} = \frac{\text{photons emitted}}{\text{photons absorbed}} = \frac{\int_{\text{emission}} P_{out}(\lambda_{em}) \frac{\lambda_{em}}{hc} d\lambda_{em}}{\int_{\text{absorption}} P_{in}(\lambda_{abs}) \frac{\lambda_{abs}}{hc} A(\lambda) d\lambda_{abs}} * 100\% \quad (3)$$

where  $P_{out}(\lambda_{em})$  is the integrated emission from all four edges over the wavelength range (in Watt). Both one parallel and one perpendicular edge were measured and multiplied by 2 to approximate the total output.  $P_{in}$  is the incident light power from the solar simulator (in Watt),  $A(\lambda)$  is the absorption of the sample (in %),  $\lambda$  is the wavelength range over which the summation is made,  $h$  is Planck's constant, and  $c$  the speed of light. The absorption of Dye 1 was integrated over the wavelength range 350–500 nm and the emission over 450–700 nm, while for Dye 2 these values were 450–650 nm and 550–800 nm, respectively. The incoming solar simulator light was integrated over the wavelength range of 350–800 nm.

The external power efficiency decreases at higher applied voltages (see Figure 4a,b) as the incident light remains constant, but the emitted light decreases due to the reduced absorption of light. The internal optical efficiency increases at higher applied voltages (see Figure 4c,d) as, despite the decrease in absorption, the light that is absorbed is emitted much more effectively towards the edges of the system due to the favorable dye alignment [23].

In many cases, it might be desirable for the 'smart' window to be in the most transparent state, and only upon increasing temperature or application of voltage should it become more absorbing. Such a device was fabricated by replacing the planar with a homeotropic alignment layer and switching from a fully ITO-coated glass substrate to an IDE-coated substrate. In this latter device, the thermal response is unchanged, while the LC and dye are switched from a homeotropic (transparent) alignment to a planar (absorbing) alignment by application of a voltage, as depicted in Figure 5. The reorientation from homeotropic to planar was confirmed by POM (Figure S2), where the initial dark images become bright upon application of a voltage until the isotropic state is reached and the image stays dark.

The transmissions at the absorption peaks of the dyes of this modified homeotropic device are shown in Figure 6. As mentioned earlier, the effect of heating are very similar to the planar device: that is, at higher temperatures the transmission decreases and the voltage required to switch the system decreases. The response to changes in potential is the opposite, however: at higher voltages, the absorption increases. The relative difference in transmission upon application of an electrical field is smaller compared to the planar ITO-coated system, most likely as the electrical field between the electrodes is less homogeneous, resulting in less uniform LC alignments. The edge emissions for the homeotropic-aligned system with IDE could not be reliably measured as the IDE cells had a very small switching area ( $1 \times 1 \text{ cm}^2$ ). However, the emission spectra of the planar ITO device with potential applied should match quite closely to the homeotropic IDE system at rest.

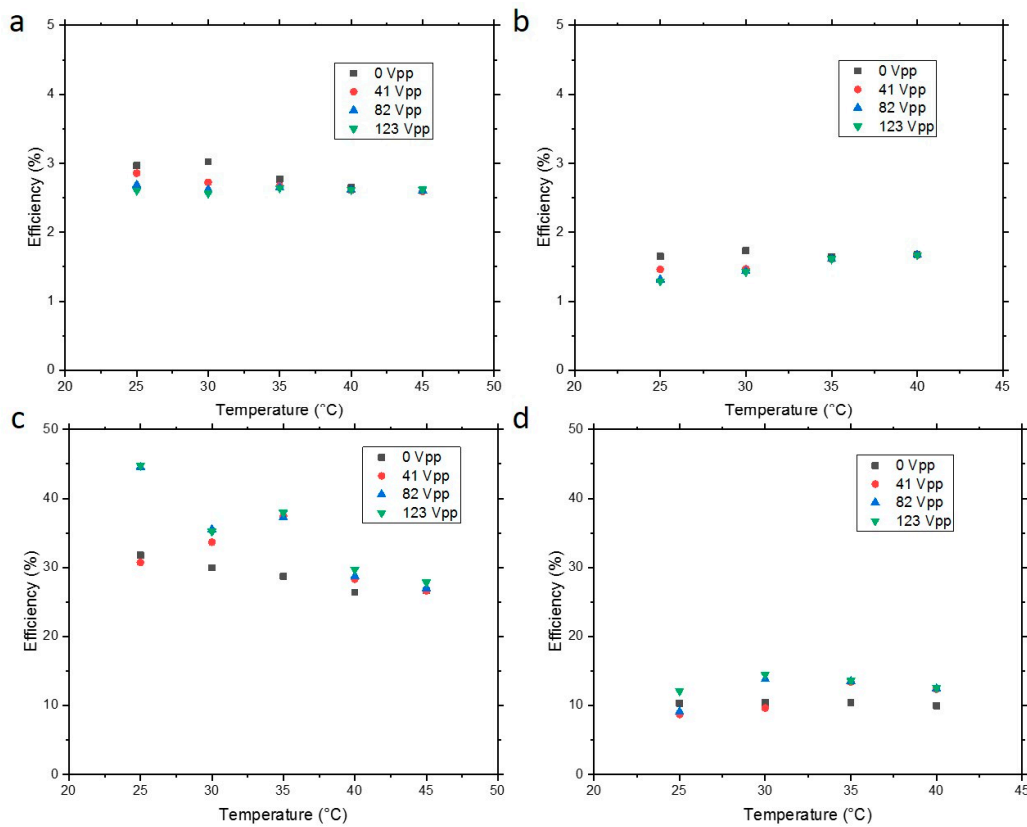


**Figure 4.** External power efficiency at different temperatures and applied electrical fields of a planar cell filled with (a) Dye 1; (b) Dye 2. Internal optical efficiency at different temperatures and applied electrical fields of a planar cell filled with (c) Dye 1; (d) Dye 2.

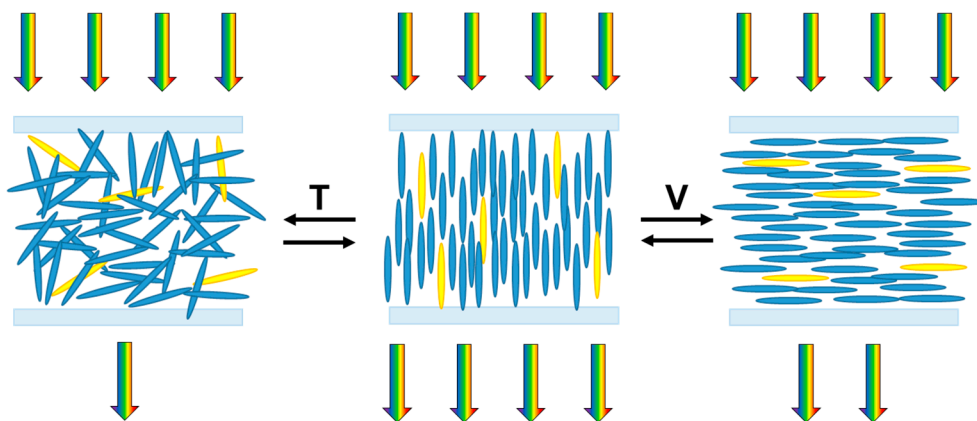


**Figure 5.** Schematic of liquid crystal and dye alignment in an initial homeotropic state (**middle**) and its changes upon application of an electrical field (**right**) or increased temperature (**left**).

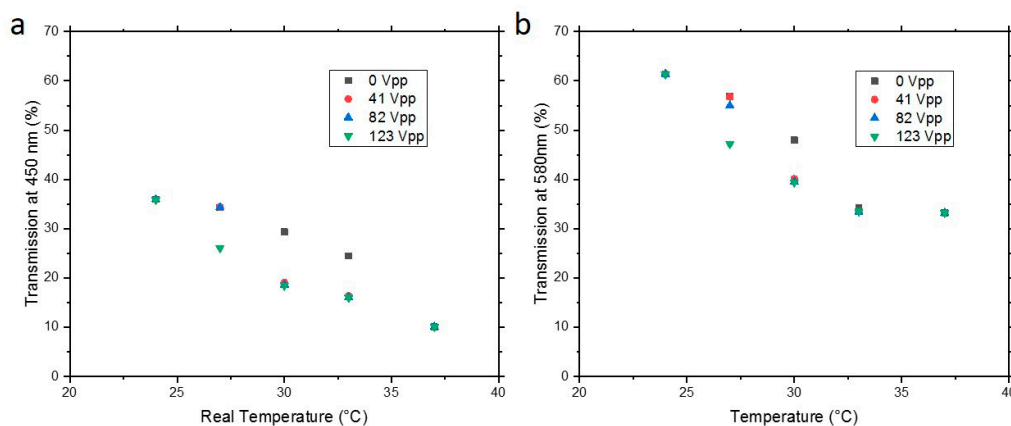


**Figure 6.** Peak transmission of an interdigitated homeotropic cell as a function of temperature and voltage filled with 8CB and 1 wt% of (a) Dye 1; (b) Dye 2.

#### 4. Discussion

Ideally, one would prefer a smart window that requires the minimum use of power to operate. In regions of the world with many hours of sunlight in buildings primarily used in daytime, like office buildings, this would be a window that is in the dark, absorbing state when switched ‘off’. However, there will also be situations where the opposite is desired: the windows remain transparent until some state at which light intensity is too high, and may then switch to absorbing, such as in a greenhouse, for example. In order to improve the performance of a smart window with a transparent rest state, rather than using an IDE cell as described in this work, an LC could be used with a negative dielectric anisotropy in an ITO cell. This combination allows switching from a transparent homeotropic-aligned system to an absorbing planar alignment by the application of a voltage [29]. The advantage would be that a simpler ITO design can be used with better switching properties, as the IDE system inhibited full switching, and its limited in-cell gap affects the maximum absorption that can be reached, as many dyes have limited solubility in the LC host. Further performance improvements can be achieved by adjusting the structures of the dyes: enhanced alignment can be achieved, resulting in a better contrast between the ‘on’ and ‘off’ states of the electrically switched system [30], and simultaneously enhancing edge emissions as well.

Deploying these switchable windows in the built environment could have several advantages. First, one can create windows that make better use of the incident sunlight, reducing light transmission and glare under bright, hot conditions and using this excess solar energy to generate power which could be used to allow the window to switch itself. Triggering window transmission changes to variations in external temperature allows switching to be done automatically, while the electrical switching allows for individuals to override the automatic temperature response. The temperature range for switching may be tuned by adjusting the LC host system, although the current device, which switches between about 25 and 35 °C, already seems appropriate.

One potential disadvantage of these LC-based devices is the reliance on the smectic phase of the LC. The smectic phase is often somewhat scattering, resulting in a slightly ‘hazy’ appearance to the window, as if it is somewhat soiled. What may be viewed as potential disadvantage in a commercial building actually becomes a positive feature with windows deployed in horticulture, for example, where the diffusing of light can assist plant growth by allowing more light to reach deeper into the plant canopy [31]. Finally, the lifetime of these ‘smart’ window type devices is always a concern. In this particular case, the lifetime will not be very extensive due to the use of the model LC host. However, liquid-crystal based devices have been deployed outdoors worldwide in the form of advertising displays and sporting scoreboards, so it is anticipated that with optimization of the LC mixture extended lifetimes appropriate for use as windows will be possible. Likewise, many organic

dyes have already exhibited extended lifetimes [32], and it is anticipated that appropriate lifetimes may be reached for the luminescent species as well.

**Supplementary Materials:** The following are available online at <http://www.mdpi.com/2076-3417/10/4/1421/s1>, Figure S1: Differential scanning calorimetry of the dye doped 8CB cells; Figure S2: Polarized optical microscopy images of a LC cell.

**Author Contributions:** Conceptualization, M.G.D.; investigation, G.H.T. and R.F.D.; resources, J.L., M.G.D. and G.H.T. wrote the manuscript in consultation with J.L. and R.F.D. All authors have read and agreed to the published version of the manuscript.

**Funding:** This research was funded by the Dutch PPS Smart Materials for Greenhouses program.

**Conflicts of Interest:** The authors declare no conflict of interest.

## References

1. Baldwin, S.; Bindewald, G.; Brown, A.; Chen, C.; Cheung, K.; Clark, C.; Cresko, J.; Crozat, M.; Daniels, J.; Edmonds, J. *Quadrennial Technology Review: An Assessment of Energy Technologies and Research Opportunities*; Technical Report; US Department of Energy: Washington, DC, USA, 2015.
2. Pérez-Lombard, L.; Ortiz, J.; Pout, C. A review on buildings energy consumption information. *Energy Build.* **2008**, *40*, 394–398. [[CrossRef](#)]
3. Ke, Y.; Chen, J.; Lin, G.; Wang, S.; Zhou, Y.; Yin, J.; Lee, P.S.; Long, Y. Smart Windows: Electro-, Thermo-, Mechano-, Photochromics, and Beyond. *Adv. Energy Mater.* **2019**, *9*, 1902066. [[CrossRef](#)]
4. Khandelwal, H.; Loonen, R.C.G.M.; Hensen, J.L.M.; Debije, M.G.; Schenning, A.P.H.J. Electrically switchable polymer stabilised broadband infrared reflectors and their potential as smart windows for energy saving in buildings. *Sci. Rep.* **2015**, *5*, 11773. [[CrossRef](#)] [[PubMed](#)]
5. Oh, S.-W.; Kim, S.-H.; Yoon, T.-H. Control of Transmittance by Thermally Induced Phase Transition in Guest-Host Liquid Crystals. *Adv. Sustain. Syst.* **2018**, *2018*, 1800066. [[CrossRef](#)]
6. Oh, S.W.; Kim, S.H.; Yoon, T.H. Thermal control of transmission property by phase transition in cholesteric liquid crystals. *J. Mater. Chem. C* **2018**, *6*, 6520–6525. [[CrossRef](#)]
7. Zhang, Y.; Tso, C.Y.; Iñigo, J.S.; Liu, S.; Miyazaki, H.; Chao, C.Y.H.; Yu, K.M. Perovskite thermochromic smart window: Advanced optical properties and low transition temperature. *Appl. Energy* **2019**, *254*, 113690. [[CrossRef](#)]
8. Khandelwal, H.; Debije, M.G.; White, T.J.; Schenning, A.P.H.J. Electrically tunable infrared reflector with adjustable bandwidth broadening up to 1100 nm. *J. Mater. Chem. A* **2016**, *4*, 6064–6069. [[CrossRef](#)]
9. Binet, C.; Mitov, M.; Mauzac, M. Switchable broadband light reflection in polymer-stabilized cholesteric liquid crystals. *J. Appl. Phys.* **2001**, *90*, 1730–1734. [[CrossRef](#)]
10. Talukder, J.R.; Lee, Y.-H.; Wu, S.-T. Photo-responsive dye-doped liquid crystals for smart windows. *Opt. Express* **2019**, *27*, 4480. [[CrossRef](#)]
11. Goda, K.; Omori, M.; Takatoh, K. Optical switching in guest–host liquid crystal devices driven by photo- and thermal isomerisation of azobenzene. *Liq. Cryst.* **2017**, *45*, 485–490. [[CrossRef](#)]
12. Oh, S.-W.; Kim, S.-H.; Baek, J.-M.; Yoon, T.-H. Optical and Thermal Switching of Liquid Crystals for Self-Shading Windows. *Adv. Sustain. Syst.* **2018**, *2*, 1700164. [[CrossRef](#)]
13. Vasiliev, M.; Alameh, K.; Nur-E-Alam, M. Spectrally-Selective Energy-Harvesting Solar Windows for Public Infrastructure Applications. *Appl. Sci.* **2018**, *8*, 849. [[CrossRef](#)]
14. Alghamedi, R.; Vasiliev, M.; Nur-E-Alam, M.; Alameh, K. Spectrally-selective all-inorganic scattering luminophores for solar energy-harvesting clear glass windows. *Sci. Rep.* **2015**, *4*, 6632. [[CrossRef](#)] [[PubMed](#)]
15. Vasiliev, M.; Alghamedi, R.; Nur-E-Alam, M.; Alameh, K. Photonic microstructures for energy-generating clear glass and net-zero energy buildings. *Sci. Rep.* **2016**, *6*, 31831. [[CrossRef](#)]
16. Debije, M.G.; Verbunt, P.P.C. Thirty Years of Luminescent Solar Concentrator Research: Solar Energy for the Built Environment. *Adv. Energy Mater.* **2012**, *2*, 12–35. [[CrossRef](#)]
17. Mckenna, B.; Evans, R.C. Towards Efficient Spectral Converters through Materials Design for Luminescent Solar Devices. *Adv. Mater.* **2017**, *29*, 1606491. [[CrossRef](#)]
18. Earp, A.A.; Smith, G.B.; Franklin, J.; Swift, P. Optimisation of a three-colour luminescent solar concentrator daylighting system. *Sol. Energy Mater. Sol. Cells* **2004**, *84*, 411–426. [[CrossRef](#)]

19. Cambi , D.; Zhao, F.; Hessel, V.; Debije, M.G.; No l, T. A Leaf-Inspired Luminescent Solar Concentrator for Energy-Efficient Continuous-Flow Photochemistry. *Angew. Chem. Int. Ed.* **2017**, *56*, 1050–1054. [[CrossRef](#)]
20. Zhao, F.; Cambi , D.; Hessel, V.; Debije, M.G.; No l, T. Real-time reaction control for solar production of chemicals under fluctuating irradiance. *Green Chem.* **2018**, *20*, 2459–2464. [[CrossRef](#)]
21. Makarov, N.S.; Ramasamy, K.; Jackson, A.; Velarde, A.; Castaneda, C.; Archuleta, N.; Hebert, D.; Bergren, M.R.; McDaniel, H. Fiber-Coupled Luminescent Concentrators for Medical Diagnostics, Agriculture, and Telecommunications. *ACS Nano* **2019**, *13*, 9112–9121. [[CrossRef](#)]
22. Sol, J.A.H.P.; Timmermans, G.H.; van Breugel, A.J.; Schenning, A.P.H.J.; Debije, M.G. Multistate Luminescent Solar Concentrator “Smart” Windows. *Adv. Energy Mater.* **2018**, *8*, 1702922. [[CrossRef](#)]
23. Debije, M.G. Solar Energy Collectors with Tunable Transmission. *Adv. Funct. Mater.* **2010**, *20*, 1498–1502. [[CrossRef](#)]
24. Wu, J.; He, D.; Wang, Y.; Su, F.; Guo, Z.; Lin, J.; Zhang, H.-J. Selective Ortho - $\pi$ -Extension of Perylene Diimides for Rylene Dyes. *Org. Lett.* **2018**, *20*, 6117–6120. [[CrossRef](#)] [[PubMed](#)]
25. Kahl, P.; Baroni, P.; Noirez, L. Hidden solidlike properties in the isotropic phase of the 8CB liquid crystal. *Phys. Rev. E* **2013**, *88*, 050501. [[CrossRef](#)] [[PubMed](#)]
26. Lub, J.; Broer, D.J.; Wegh, R.T.; Peeters, E.; van der Zande, B.M. Formation of Optical Films by Photo-Polymerisation of Liquid Crystalline Acrylates and Application of These Films in Liquid Crystal Display Technology. *Mol. Cryst. Liq. Cryst.* **2005**, *429*, 77–99. [[CrossRef](#)]
27. Bose, T.K.; Campbell, B.; Yagihara, S.; Thoen, J. Dielectric-relaxation study of alkylcyanobiphenyl liquid crystals using time-domain spectroscopy. *Phys. Rev. A* **1987**, *36*, 5767–5773. [[CrossRef](#)]
28. Tummeltshammer, C.; Taylor, A.; Kenyon, A.J.; Papakonstantinou, I. Losses in luminescent solar concentrators unveiled. *Sol. Energy Mater. Sol. Cells* **2016**, *144*, 40–47. [[CrossRef](#)]
29. Crooker, P.P.; Yang, D.K. Polymer-dispersed chiral liquid crystal color display. *Appl. Phys. Lett.* **1990**, *57*, 2529–2531. [[CrossRef](#)]
30. Kendhale, A.M.; Schenning, A.P.H.J.; Debije, M.G. Superior alignment of multi-chromophoric perylenebisimides in nematic liquid crystals and their application in switchable optical waveguides. *J. Mater. Chem. A* **2013**, *1*, 229–232. [[CrossRef](#)]
31. Hemming, S.; Dueck, T.A.; Janse, J.; van Noort, F. The effect of diffuse light on crops. *Acta Hortic.* **2008**, *801*, 1293–1300. [[CrossRef](#)]
32. Baumberg, I.; Berezin, O.; Drabkin, A.; Gorelik, B.; Kogan, L.; Voskoboynik, M.; Zaidman, M. Effect of polymer matrix on photo-stability of photo-luminescent dyes in multi-layer polymeric structures. *Polym. Degrad. Stab.* **2001**, *73*, 403–410. [[CrossRef](#)]



  2020 by the authors. Licensee MDPI, Basel, Switzerland. This article is an open access article distributed under the terms and conditions of the Creative Commons Attribution (CC BY) license (<http://creativecommons.org/licenses/by/4.0/>).